

OPTICAL MICROSCOPY

PACS numbers: 07.79.Fc
DOI: 10.1070/QE2007v037n02ABEH008955

Scanning near-field optical microscopy and near-field optical probes: properties, fabrication, and control of parameters

V.F. Dryakhlushin, V.P. Veiko, N.B. Voznesenskii

Abstract. **A brief review of modern applications of scanning near-field optical (SNO) devices in microscopy, spectroscopy, and lithography is presented in the introduction. The problem of the development of SNO probes, as the most important elements of SNO devices determining their resolution and efficiency, is discussed. Based on the works of the authors, two different methods for fabricating SNO probes by using the adiabatic tapering of an optical fibre are considered: the laser-heated mechanical drawing and chemical etching. A nondestructive optical method for controlling the nanometre aperture of SNO probes is proposed, substantiated, and tested experimentally. The method is based on the reconstruction of a near-field source with the help of a theoretical algorithm of the inverse problem from the experimental far-filed intensity distribution. Some prospects for a further refinement of the construction and technology of SNO probes are discussed.**

Keywords: *near-field optics, microscopy, spectroscopy, lithography*.

1. Introduction

High-resolution optical imaging was always urgent for a variety of investigations. This became especially important in the last years due to the rapid development of micro- and nanoelectronics, microbiology, physics of various nanostructures, etc. However, the possibilities of traditional optics do not already satisfy researchers. The resolution of optical methods is restricted by the diffraction limit and cannot exceed $1.22\lambda/2n$ (where λ is the light wavelength and n is the refractive index of a medium). The creation of a scanning electron microscope (SEM) solved this problem only partially because this microscope can be used only to study conducting samples. In addition, samples are studied in a SEM in a high vacuum, which complicates some applications, in particular, *in vivo* studies in microbiology. A decisive step in the study of physical phenomena was made two decades ago, when a new generation of imaging systems based on the detection and use of nonradiative fields was created: a scanning tunnelling microscope (STM), an atomic force microscope (AFM), a scanning near-field optical microscope (SNOM), and some other devices. A scanning near-field optical microscope was built soon after the advent of a scanning tunnelling microscope [1 – 3].

The operation principle of a SNOM, as of other scanning probe microscopes, is based on the scan of a sample surface by a source (or a detector) of optical radiation of size much smaller than the light wavelength, which is located at a small distance from the surface (in the near field of radiation). This makes it possible to overcome the diffraction limit because in this case the resolution is no longer dependent on the wavelength. The SNOM differs from the STM and AFM in that it requires the independent system for delivering and holding a probe near the sample surface. For this reason, as a rule, the SNOM is combined with the AFM, which provides the retaining of the probe near the surface by the so-called shear-force method [4]. This complicates the SNOM and makes it more expensive, but on the other hand, allows one to obtain simultaneously the SNOM and AFM images, which gives more complete information on the sample surface.

Being inferior to the STM and AFM in resolution, the SNOM is applied in scientific studies not only for high-resolution optical imaging but first of all in the local optical spectroscopy of microbiological and semiconductor objects, in lithography, and for surface modification for superdense data storage.

There exist different SNOM modifications. First of all, this is a classical variant in which the probe is a source of optical radiation transmitted through a sample and detected with a photodetector (illumination transmission mode) [5]. The photodetector can be located on the same side of the sample as the probe and detect a signal reflected from the sample (illumination reflection mode) [6, 7]. In other modifications, the SNOM probe is a point detector of optical radiation whose macroscopic beam is incident either on the sample surface near which the probe is located (collection reflection mode) or on the opposite side (collection transmission mode) [8, 9]. The operation principle of the so-called scanning tunnelling optical microscope [10], in which radiation is incident on a sample through a prism at the total internal reflection angle, is substantially different. The evanescent wave produced on the sample surface is transformed by the SNOM probe to a mode, which propagates in it and arrives at the photodetector. 'Low-noise' lasers are used, as a rule, as radiation sources, and radiation is detected with photomultipliers. Various SNOM designs are described in detail in review [11].

V.F. Dryakhlushin, V.P. Veiko, N.B. Voznesenskii St. Petersburg State University of Information Technologies, Mechanics and Optics, Kronverkskii prosp. 14, 197101 St. Petersburg, Russia;
e-mail: veiko@lastech.ifmo.ru, vnb@aco.ifmo.ru

Received 29 March 2005; revision received 29 May 2006
Kvantovaya Elektronika **37** (2) 193 – 203 (2007)
Translated by M.N. Sapozhnikov

Of special interest is a scanning aperture-free interference microscope (SAFIM), which provides imaging with the resolution down to 1 nm [12–14]. The principle of its operation is based on measuring the interference of the reference wave and optical wave reflected from the AFM probe. This requires extremely accurate phase measurements (with an accuracy to 10^{-7} rad $Hz^{-1/2}$), and a very complex system for signal separation is needed. It seems that for this reason the SAFIM did find wide applications despite the excellent results obtained in experiments.

The SNOM provided a drastic improvement in the resolution of optical images. At present the record resolution down to 12 nm ($\lambda/43$) was obtained by using this microscope [15], which is considerably lower than the diffraction limit. Several research groups achieved the resolution of ~ 30 nm. This made it possible to obtain optical images of various objects such as large organic molecules, viruses, and individual elements of micro- and nanoelectronic devices, which cannot be imaged by traditional optical methods. The development of near-field optics stimulated the appearance of new fields of scientific research such as local spectroscopy and local surface modification with the resolution 30–100 nm.

The local SNOM modification of surfaces [near-field (NF) lithography] can find applications for superdense data storage and in the development of nanoelectronic devices. Direct near-field optical lithography with the use of photoresists allows one to obtain figures with the size of the minimal resolved element as small as 100 nm [16, 17] because of a rapid decrease in the transmission coefficient of the probe (proportional to a^6 [5], where a is the probe aperture). In our opinion, more interesting results were obtained upon the direct action of radiation emerging from the SNOM probe on the surface of some samples. In [18], the possibility of reverse data recording and reading with the help of small magnetooptical domains was studied. Phase changes in a GeSbTe semiconductor film were investigated in [19]. The minimal size of the information bit in this experiment was 60 nm, which corresponds to the data storage density ~ 28 Gbit cm^{-2}. The SNOM modification of different organic films was studied in [20, 21], where individual elements of size ~ 70 nm were obtained. Experimental results show that the data recording density can exceed 16 Gbit cm^{-2} and the reading rate can exceed 1 Mbit s^{-1}.

Another NF lithography method for fabricating nanometre elements for nanoelectronic devices was proposed in [22]. The method involves the deposition of a thin two-layer polymer–metal film coating, the non-plastic deformation of the upper metal layer by a heated SNOM probe, the transfer of a figure via the polymer on the sample surface with the help of dry etching, and the fabrication of various nanometre elements through a mask prepared in this way. By using this method, arbitrary pictures can be produced on the surface of various samples (etched pits, grooves, metal and dielectric dots, lines and their combinations). Lateral elements of size 30–50 nm can be manufactured.

Scanning near-field optical spectroscopy, being another scientific field based on SNOM applications, is an extremely useful tool for studying the local properties of physical, microbiological, and chemical objects with a resolution not exceeding 100 nm [23–26]. It is widely used in microbiology to investigate the properties of individual viruses, neurons, large organic molecules *in vivo*, in particular, their fluorescence and polarisation [27, 28]. The possibility of the local modification of single microbiological objects or their elements is also attractive (gene engineering). Several remarkable results were obtained in SNOM studies [12] of individual organic molecules and viruses with the resolution of ~ 5 nm [29].

Scanning near-field optical spectroscopy offers unique possibilities for studying semiconductor nanoobjects such as quantum wells [30], wires [31], and dots [32, 33]. This method is used sometimes in combination with picosecond [34] and femtosecond [31] techniques. The energy spectra of single quantum nanoobjects, times and diffusion lengths of minority charge carriers, emission and transport of excitons were studied. Various mutually complementary results were obtained in measurements performed in the illumination and collection modes. Another method for studying nanostructures is the method of near-field photoconductivity in which a SNOM probe is scanned along the structure cleavage, exciting locally charge carriers [35]. This method allows the measurement of the energy and geometrical parameters of a heterostructure and of the diffusion length of minority charge carriers. The possibility of mapping emitting surfaces of semiconductor lasers is important for practical applications. Experiments were performed both with usual lasers [36, 37] and vertical-cavity surface-emitting lasers [38]. The method of near-field photoconductivity can be used to determine the near-field spatial and spectral distributions of radiation modes and to find defects of a semiconductor structure. Note also the possibility of direct observations of scattering [39] and SHG [40] of surface plasmons propagating along a rough surface. The technique of scanning near-field optical microscopy is applied for studying submicron semiconductor structures, interfaces in semiconductors, etc. by exciting photocurrent and analysing the parameters of semiconductors by spectroscopic methods [37].

A probe is a key element of a SNOM. The probe aperture determines the resolution of the microscope and its efficiency limits the optical power propagating through the probe, which determines the possibilities of SNOM applications for surface modification and in high-spatial resolution spectroscopy.

There exist several types of SNOM probes. The most promising and often used is a probe based on an adiabatically tapered single-mode optical fibre covered by a thin metal film and having a small-aperture point [41]. The optical fibre should be single-mode to provide the efficient conversion of its fundamental HE_{11} mode to the TE_{11} mode of a cylindrical metal waveguide having the smallest critical diameter. For a cylindrical metal waveguide filled with quartz, the critical diameter for the radiation wavelength 0.5 μm is 0.21 μm for the TE_{11} mode and increases up to 0.28 and 0.35 for the two next modes [42]. Thus, the higher radiation modes propagate through the aperture considerably weaker. The tapering angle of the probe substantially determines its parameters. On the one hand, the tapering angle should be rather gradual (to reduce reflection and provide a better localisation of a light wave), and on the other, too slow tapering leads to an increase in ohmic losses on the probe walls. It is accepted that the optimal tapering angle is $\sim 10^\circ$ between the fibre axis and its boundary. Probes are manufactured either by the method of temperature-controlled mechanical drawing of an optical fibre [42] or by chemical etching of fibres [43].

Another variant of the SNOM probe used at present is manufactured based on a silicon AFM edge-lever [40]. A sharp pyramid (with the apex angle 56°) is etched on the edge-lever surface by the method of anisotropic etching. The pyramid is covered with a thin metal layer, except for a small aperture at the apex, and then silicon is removed from under metal. During microscope operation, radiation is focused by an optical system on the aperture. The advantage of this probe over fibre probes is that high radiation powers can be introduced into it (due to efficient heat removal), while its disadvantage is the absence of a gradual localisation of radiation, which reduces the transmission coefficient. In addition, it is necessary to focus accurately optical radiation on the probe aperture, which complicates the operation procedure. As a result, probes based on optical fibres are used more often [44–46]. Note also studies devoted to the creation of point photodetectors integrated with the AFM edge-lever for operation in the collection mode [46].

The SNOM probe determines both the resolution of the microscope and the possibility of its various applications, and studies devoted to the improvement of probes available and the development of probes based on new principles are proceeding very actively. The possibilities of a further development and applications of the near-field techniques are also considerably restricted by the problem of interpretation of near-field images obtained in experiments. This problem appears first of all because it is impossible to determine *a priori* the size and shape of the aperture of a near-field optical probe (NOP). In this paper, we consider various methods of manufacturing and studying SNOM probes and discuss the prospects for the development of probes with qualitatively better electrodynamic parameters. We also consider the possibility of determining the instrumental function of fibreoptic NOPs and substantiate the principles of optical control and testing of probes providing information on their optical properties.

2. Laser technology for manufacturing near-field optical probes

In most cases a NOP represents a tapered optical fibre with the tapered end of size that is much smaller than the light wavelength (~ 100 nm). Near-field probes are manufactured at present either by chemical etching or mechanical drawing of a local part of the fibre heated to the viscous-fluid state. The SNOM resolution and its efficiency are mainly determined by the NOP parameters. Consider first the manufacturing of NOPs by drawing from a laser-heated optical fibre. To manufacture probes with the specified parameters and obtain good reproducibility of the results, it is necessary to know the main parameters of the drawing process. The kinetics of mechanical drawing of laser-heated optical fibres and the properties of formation of the NOP geometry were studied in [47, 48]. The laser-assisted drawing of silica fibres is performed by heating fibres with the 10.6-μm radiation from a CO_2 laser of power up to 20 W, which falls into the fundamental absorption band of silica. The laser drawing method is most often used among 'thermal' methods, and one of its main advantages is the high efficiency. However, the control of drawing parameters during the drawing process is quite complicated due to the high drawing rate.

The main technological parameters are the elongation of the heated part of the fibre and the change of its temperature with time. Even small temperature variations during the drawing process can change the geometrical parameters of the NOP being formed.

The NOP shape strongly depends on the symmetry of a heat source formed on the fibre surface due to absorption of laser radiation. Therefore, to optimise the laser-assisted fibre drawing, it is necessary to use an optical scheme for radiation focusing capable of providing the uniform circular illumination of a local site of the fibre. Such a scheme was developed, experimentally tested and described in [47]. The main element of the scheme is a spherical mirror providing the production of a circular heat source in the fibre (Fig. 1a). The mechanical part of the setup contains a mechanism to draw the fibre in the horizontal plane.

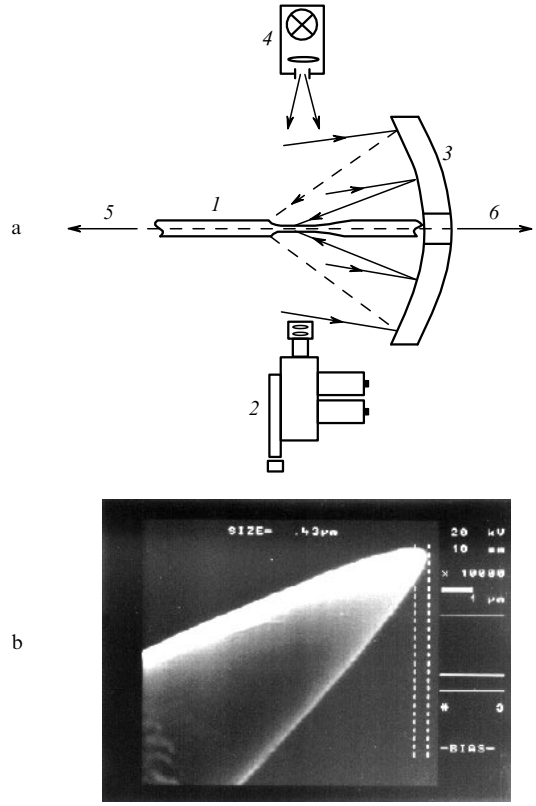

Figure 1. Scheme for manufacturing a NOP by laser-assisted drawing: [(*1*) optical fibre; (*2*) SKS-1M high-speed camera; (*3*) spherical mirror; (*4*) illuminating system; arrows (*5*) and (*6*) show the direction of fibre stretching] (a) and photograph of the probe (b).

The setup was used to fabricate probes with submicron tapered ends drawn from a single-mode silicon fibre (with the core diameter of 9.5 μm and silica cladding diameter of 125 μm). The photograph of such a probe is shown in Fig. 1b. The setup was then used to study the kinetics of laser-assisted fibre drawing and variation in the fibre temperature during the drawing process.

The technology of laser-assisted drawing of NOPs is well developed (see, for example, [8]). However, the optimisation of this technology requires more detailed studies of the laser heating and fibre elongation kinetics, which has not been adequately considered in the literature so far. We used for this purpose two methods: rapid filming and two-wave spectral-ratio pyrometry.

The NOP drawing kinetics was studied by the rapid filming method by using an SKS-1M camera. The filming was performed with the fivefold magnification at the rate of 600 – 1000 frames per second.

We studied visually the drawing process by this method, determined its main stages, measured the total time of the process (from the onset of fibre heating to its rupture at the tapered part accompanied by the formation of tapered fibre ends), measured the diameter and elongation of tapered fibre ends, and investigated the influence of variations in the laser radiation power on the formation of microscopic tapered fibre ends, etc.,

The laser-assisted drawing process can be conventionally divided into four main stages (see Fig. 2):

(i) A comparatively long fibre heating (for the time $t \approx 0.15$ s) during which no noticeable changes in the fibre diameter occur;

(ii) a small smooth tapering of the heated fibre region ($t \approx 0.15 - 0.23$ s);

(iii) a rapid decrease in the fibre diameter during the maximum heating of the fibre in the focus of a spherical mirror ($t \approx 0.23 - 0.26$ s);

(iv) the fibre rupture with the formation of tapered ends.

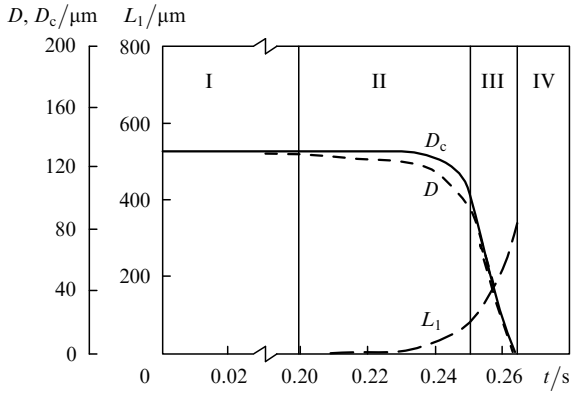

Figure 2. The dependences of the geometrical parameters of NOP points produced during laser-assisted drawing (I – VI: stages of the drawing process).

The filming data give the time dependences of the minimal fibre diameter D in the heated region (Fig. 2) and of tapered end lengths L_1. The tapered fibre ends were measured during drawing from the point of the lowest diameter of the thin fibre waist to the point with $D =$ 125 μm.

The experimental data obtained in our study confirm the results of theoretical analysis of the laser-assisted drawing process and the mathematic model based on the Newton law of viscous flow taking into account the temperature dependence of the viscosity. The basic concepts of the model are presented in [48]. Figure 2 also shows the calculated dependence $D_c(t)$.

The drawing of tapered silica fibre ends is a rather complicated technological process because the softening temperature of silica is high. The melting temperature at which silica transforms to liquid and can evaporate efficiently is somewhat higher. The drawing of tapered fibre ends should be performed within a narrow temperature interval, which presents some technological problems. If the fibre temperature becomes lower than the softening temperature during the drawing process, this will result in the hardening and cleavage of fibre ends before their final diameter will achieve the nanometre size. If the fibre temperature is close to the vaporisation temperature and the fibre material passes to the liquid phase, the action of gravitational forces on the melted volume becomes efficient and the drawing of tapered fibre ends will occur with the distortion of their shape. It is especially difficult to maintain the required temperature from the instant when the fibre diameter in the heated region becomes comparable with the CO_2 laser wavelength and scattering of radiation becomes noticeable [49].

Thus, it is very important to control accurately the temperature of a silica fibre during drawing tapered ends. The fibre temperature was measured during drawing by the method of spectral-ratio pyrometry [50, 51]. This method allows one to determine very accurately the temperature of the heated region in the temperature range where the softening of silica begins and the fibre diameter decreases during fibre stretching.

The operation of spectral-ratio pyrometers is based on the fact that the maximum of the thermal emission band of a body shifts to the blue with increasing temperature. Therefore, the radiation intensity ratio at two wavelengths (λ_1 and λ_2) will depend on temperature.

We obtained the experimental dependence of the fibre temperature on time during the laser-assisted drawing of NOP points (Fig. 3). The curve in Fig. 3 is plotted assuming that silica can be treated as a grey body for which the radiating capacity is constant over the spectrum [i.e.$\varepsilon_1(\lambda_1) = \varepsilon_2(\lambda_2)$] and, therefore, its colour temperature is equal to the thermodynamic temperature. Figure 3 illustrates the drawing process of duration 0.19 s. This time is well consistent with the rapid filming data obtained under similar experimental conditions.

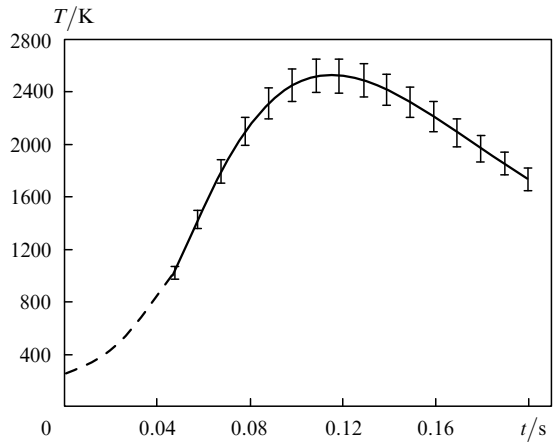

Figure 3. Time dependence of the temperature of the heated region of a silica fibre during the laser-assisted drawing of NOP points.

One can see from Fig. 3 that the fibre temperature in the heated region at the beginning of drawing starts to increase drastically, achieving ~ 2500 K, and then some stabilisation occurs, which is accompanied by a weak decrease in temperature. The stabilisation occurs because the total amount of energy lost due to the convective cooling of the fibre and displacement of the heated region (inherent in the given optical scheme) becomes equal to the energy

absorbed by the fibre. It seems that the total length of the tapered fibre end obtained upon drawing is independent of the length of this part of the curve. Then, the fibre temperature in the stretched region begins to drop. This occurs due to the decrease in the fibre diameter down to the value comparable with the CO_2 laser wavelength, and radiation scattering begins to affect the fibre heating. The decrease in the fibre temperature leads to the increase in the silica viscosity, resulting in the fibre rupture in its thinnest part at temperature 1600 K. The fibre rupture at low temperature favours drawing because in this case the melting of the tapered fibre end caused by surface tension forces, which could reduce the transmission coefficient and efficiency of the NOP, can be avoided.

The alternative method of manufacturing NOPs is the method of chemical etching.

3. SNOM probes manufactured by the method of chemical etching

The method for manufacturing SNOM probes based only on the chemical etching of an optical fibre was proposed in [39]. We improved this technique. The main advantage of probes fabricated by chemical etching is that the fibre core comes to the probe aperture. In a mechanically drawn fibre, the fibre core quite rapidly ceases to confine radiation at the fibre centre, and radiation propagates in a superdimensional waveguide, which results in the radiation transfer to higher modes. This disadvantage is absent in probes fabricated by chemical etching of optical fibres. In addition, we fabricated probes from fibres with a small-diameter core and, hence, a small (less than 5 μm) localisation region of radiation. All these provide the more efficient conversion of the HE_{11} mode of a single-mode optical fibre to the TE_{11} mode of a cylindrical metal waveguide. The preservation of the core in the fibre during fabrication of the probe also improves the concentration of optical radiation in the tapered region of the fibre, thereby reducing ohmic losses on the metal waveguide walls. As a result, probes manufactured by chemical etching have the transmission coefficient equal to $(10^{-2} - 3) \times 10^{-4}$, which is two–three orders of magnitude higher than that for probes fabricated by mechanical drawing.

A probe was manufactured by placing a preliminary cleaned fibre into a vessel filled with two immiscible liquids. A liquid that does not interact with the fibre (toluene) was located over the etching mixture (hydrofluoric acid, ammonia fluoride, and water in the proportion 10 : 1 : 10). At the liquid interface on the fibre surface, a meniscus is formed whose height changes upon variation in the fibre diameter during etching. This is accompanied by the formation of a cone at the liquid interface. By selecting liquids wetting the fibre differently, we can form a cone with the required tapering angle. The etching rate in our experiments was ~ 2.5 μm min^{-1}.

The size of the point of cones manufactured by this method did not exceed 100 nm. To fabricate cones with smaller points (and, hence, probed with a smaller aperture), the fibre was immersed into the $HF : NH_4F : H_2O = 1 : 10 : 120$ mixture, where etching was performed at the rate 0.2 μm min^{-1}. As a result, the cone point size was reduced down to 30 nm.

Figure 4 shows the SEM image of the tapered fibre end covered with a thin ($\sim$ 10 nm) metal film. Then, a thin two-layer metal film is deposited on the sharpened fibre by the method of electron-beam evaporation in vacuum. The angle between the fibre axis and the metal escape direction is $\sim 20^{\circ}$; as a result, a small aperture remains on the cone point located in a 'shadow'. As a rule, a two-layer coating, consisting of vanadium ($\sim$ 20 nm) and aluminium ($\sim$ 70 nm), is used. These metals were chosen because vanadium has good adhesion to silica, while aluminium has a thin skin layer for visible radiation ($\sim$ 7 nm). The SEM image of the SNOM probe is shown in Fig. 5. The reproducibility of this method is $\sim 90\,\%$.

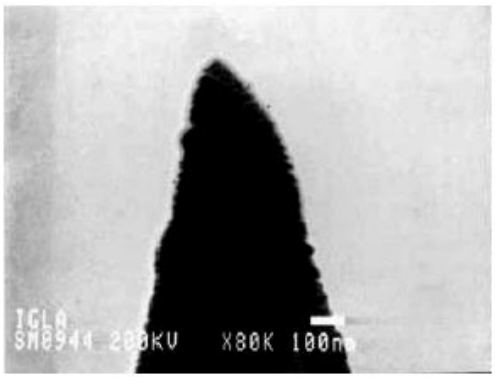

Figure 4. SEM image of a tapered optical fibre.

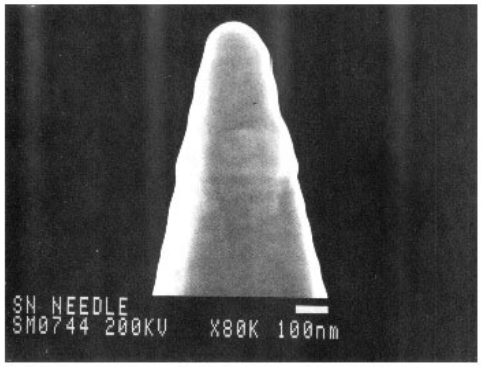

Figure 5. SEM image of a SNOM probe.

We fabricated SNOM probes with transmission coefficients of $10^{-2} - 10^{-3}$ for green light ($\lambda = 0.48 - 0.56$ μm), $5 \times 10^{-3} - 5 \times 10^{-4}$ for red light (0.60–0.68 μm), and $2 \times 10^{-3} - 2 \times 10^{-4}$ for IR light (0.78–1.05 μm).

The SNOM probes fabricated by chemical etching offer the following advantages:

(i) The optical fibre core comes to the probe aperture. This improves the localisation of optical radiation in the tapered region of the fibre, thereby increasing the transmission coefficient and reducing ohmic losses on the metal waveguide walls, i.e. reducing heating.

(ii) this method of manufacturing of SNOM probes does not require the expensive equipment.

Figure 6 shows the SNOM image of a test object [very thin ($\sim$ 10 nm) vanadium film on a quartz substrate partially etched to the substrate]. The transmission coefficient of this probe at 0.63 μm is 4×10^{-3} and the minimal resolvable image element does not exceed 40 nm.

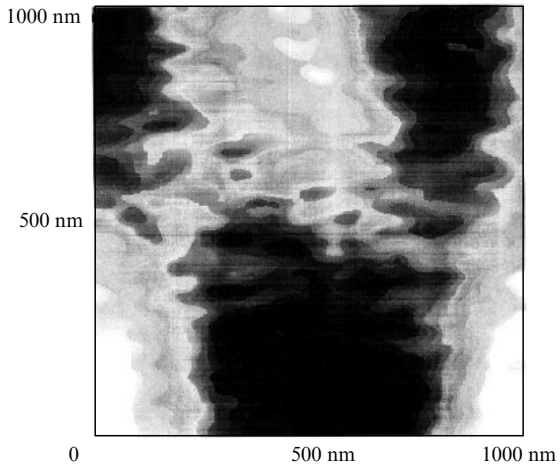

Figure 6. SNOM image of a test object.

It is necessary to mention studies [52, 53] on the fabrication of probes with the two- and three-stage tapering of optical fibres, which reduces the region where a wave decays exponentially in an evanescent metal waveguide, thereby increasing the transmission coefficient of the probe.

The problem of the nondestructive (and non-traumatic) on-line control of NOPs has not been solved so far. The NOP aperture is usually measured by using a SEM, and the probe cannot be used in a SNOM after these measurements. However, the probe aperture and efficiency can be measured directly in a SNOM by using etalon samples. Nevertheless, the independent on-line control of NOPs or their control immediately after fabrication is extremely important for their attestation and improvement of the manufacturing technology.

Below, we propose and realise a promising approach to this problem based on the recording of the far-field NOP radiation distribution and the theoretical reconstruction of the NOP aperture by solving the inverse diffraction problem.

4. Determination of the instrumental function of fibreoptic SNOM probes from experimental far-field angular light intensity distributions

It follows from the diffraction theory [54] that electromagnetic-field distributions in the near- and far-field diffraction zones are interrelated, which allows one to solve the inverse problems of diffraction and optical superresolution if the corresponding *a priori* data are available.

The necessity of solving inverse problems of this type appeared in near-field optics due to the difficulties encountered in accurate studies of the subwave aperture at the end of SNOM probes manufactured from optical fibres. This aperture cannot be distinguished in a usual optical microscope, whereas other methods of high-resolution microscopy (electron scanning microscopy, atomic force microscopy, etc.) cannot give unambiguous information due to their non-optical nature. One of the methods providing the required information is the study of SNOM probes by the parameters of far-field light intensity distribution [55, 56].

The interrelation between the near and far fields can be established by describing the propagation and diffraction of a light field by subwave structures by introducing the inhomogeneous scalar potential $\tilde{f}_e$ defined taking into account the polarisation of radiation [57–59]. The distribution of the far-field amplitude is expressed most rigorously in terms of the spatial-frequency spectrum of the potential $\tilde{f}_e$, which can be also represented in the angular measurement. The description of the relation between the field distribution produced in the plane of the probe aperture and the far-field intensity is independent of the parameters of an object from which diffraction occurred. This circumstance is used in our paper to reconstruct the near-field intensity distribution in the probe aperture plane from the far-field intensity distribution.

Let us assume for simplicity that the probe aperture is a hole in a thin metal screen. In the plane of this screen, from its rear side, the scattered field appears, which is produced by radiation incident on the screen from the frontal side and by the induced currents, which in turn produce an alternating electromagnetic field. As a result, the electromagnetic field with the characteristic size of the spatial structure smaller than the incident light wavelength appears in a medium near the screen. This field forms the main part of the so-called near field consisting of inhomogeneous plane waves, which rapidly decay in the direction perpendicular to the screen [54]. However, the waves of the near field propagate from the hole along the screen surface by large distances (theoretically, to infinity), and the law of conservation of energy is manifested in a gradual and extremely slow decay of these waves.

The far-field energy propagates correspondingly to the far-field diffraction zone and is detected with a detector. A comparison of experimental data with simulated distributions shows that the increase in the conducton and thickness of the screen leads to more homogeneous far-field intensity distributions over angular coordinates. When the conduction is limited or the screen thickness is reduced, the wave propagating normally from the screen becomes dominant, while the fraction of radiation in other directions rapidly decreases. The angular intensity distribution being simulated is described by a Gaussian and does not vanish within the solid angle $\pm 90^\circ$.

Figure 7 shows the model far- and near-field light intensity distributions in the case of diffraction from the aperture of diameter 140 nm taking into account that the screen has a finite conduction [60].

The consideration of a finite conduction of the screen results in the difference of far-field intensity distributions from idealised pictures known from the classical course of the vector diffraction of light, which give a infinitely strong scattering of the diffracted field in the polarisation direction [54].

The problems of reconstruction of the size and shape of subwave objects from the far-field radiation intensity distribution require *a priori* data for their unambiguous solution. In our case, such data are the subwave size of the hole and its simple shape (circle or ellipse), a small phase difference of the waves emerging from the probe, and the knowledge of the direction of radiation polarisation.

The reconstruction problem is solved by using the analytic continuation of unknown (nonradiative) parts of the Fourier spectrum of the scalar potential $\tilde{f}_{e0}$ of the radiation field propagated through the hole to extend the definition of the parameters of near-field components – the

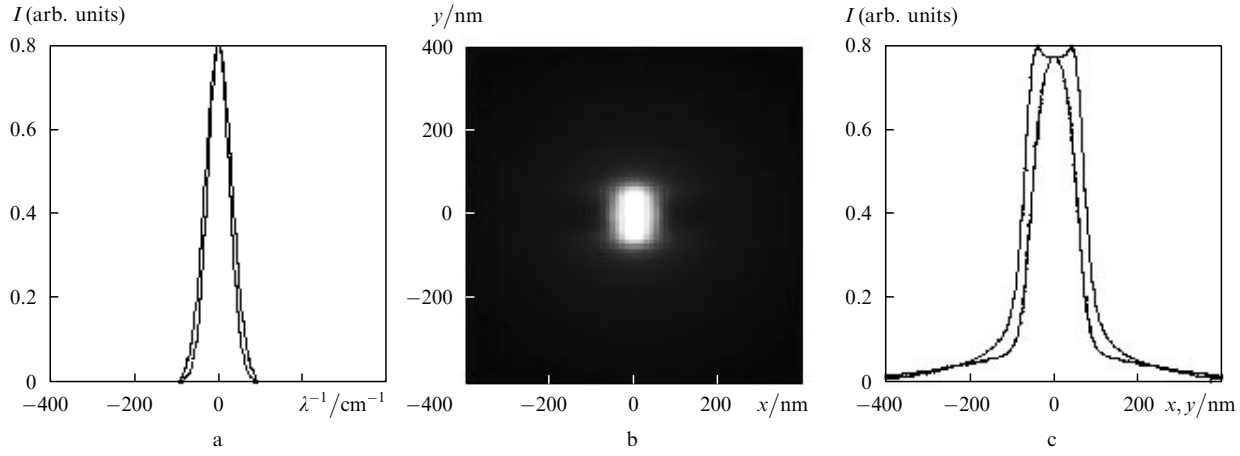

Figure 7. Transverse sections of the far-field intensity distribution of radiation diffracted from the 140-nm aperture (a), the half-tone near-field intensity distribution (b), and near-field sections (c) for the 140-nm aperture.

inhomogeneous plane waves. The analytically continued Fourier spectrum of the scalar potential $\tilde{f}_{e0}$ contains information on the shape of the hole of size of fractions of the wavelength.

As the basis functions for the analytic continuation of the spectrum, we used the two-dimensional functions of reference in the form [61–63]

$$\tilde{f}_{re}(v_x, v_y) = \sum_i \sum_j f_{ij} \sin c\left(\frac{v_x - i}{\Delta v_x}, \frac{v_y - j}{\Delta v_y}\right),$$

where $\tilde{f}_{re}$ is the spectrum being reconstructed; f_{ij} are the coefficients of expansion of the spectrum as a series in the functions of reference

$$\sin c\left(\frac{v_x - i}{\Delta v_x}, \frac{v_y - j}{\Delta v_y}\right);$$

and Δv_x and Δv_y are parameters whose values are selected to obtain the best fit.

The important problem in the construction of the algorithm for calculating coefficients f_{ij} is the formation of a criterion for analytic continuation. Usually, such a criterion in the superresolution problems is determined in the object space by the threshold intensity of unimportant details, which can be neglected. In the given case, the criterion is defined in the Fourier spectrum space in the form

$$\iint_\Omega |\tilde{f}_{rem} - \tilde{f}_{e0}|^2 \mathrm{d}v_x \mathrm{d}v_y \Big/ \iint_\Omega |\tilde{f}_{e0}|^2 \mathrm{d}v_x \mathrm{d}v_y \leqslant \varepsilon_s,$$

where ε_s is the selected threshold value; $\tilde{f}_{rem}$ is the radiative part of the mth iteration of the analytically continued Fourier spectrum of the scalar potential of the diffracted field; $\tilde{f}_{e0}$ is the measured spectrum; and Ω is the integration region. As follows from computer studies, such a criterion operates quite stably in the presence of the Gaussian noise with the root-mean-square deviation from the maximum far-field intensity equal to 10 %.

To obtain information on the far-field intensity distribution, it is sufficient to record the angular intensity distribution because upon diffraction from subwave apertures, the phase change within the solid angle $\pm 90^\circ$ is negligible. The main difficulty of recording the far-filed radiation is related to its low brightness, which was considered earlier an insurmountable problem. However, modern fibreoptic SNOM probes have the light efficiency of no less than 10^{-4} and the radiation power at the probe output achieves a few milliwatts, which allows the use of standard CCD detectors in scientific studies. In particular, CCD arrays with the signal-to-noise ratio from 56 to 62 dB and sensitivity ~ 1 lx at a wavelength of 632.8 nm can be employed.

The intensity distribution over the angular coordinate can be recorded by using either the angular scan of a photodetector with an aperture or a scheme for the simultaneous recording of the entire field in the solid angle up to 180°. In this paper, we used the results of measurements obtained by using a spherical mirror.

Figure 8 shows the scheme of the setup for measuring the far-field intensity distribution with the acceptance angle no less than $\pm 87^\circ$. The angular intensity distribution of radiation emerging from the probe is 'projected' on the CCD detector plane. Note that the relation between the linear distribution of illumination over the CCD area and the angular distribution of the probe radiation intensity should be described in this scheme by taking into account the spherical aberration of the mirror.

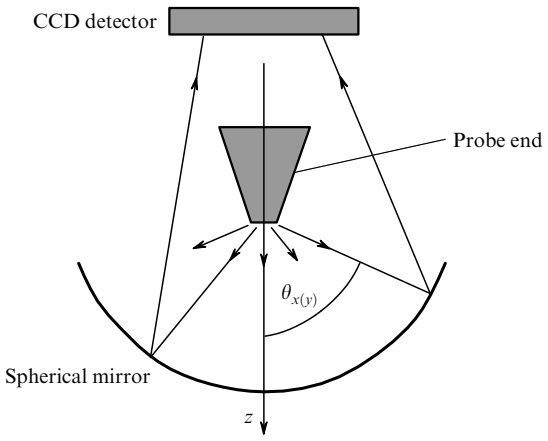

Figure 8. Scheme for recording the far-field intensity distribution with the acceptance angle no less than $\pm 87^\circ$.

Although this scheme seems quite simple, it requires the use of a special procedure of replacing apertures near the CCD detector (not shown in Fig. 8) because the direction cosines of the beam (plane waves) reflected from the mirror are nonlinearly coupled with the corresponding direction cosines of plane waves emerging from the probe and incident on the mirror. Therefore, the measurement 'field' should be divided into zones in which the angular coordinates on the CCD detector can be unambiguously identified.

Figures 9 and 10 illustrate the stages of processing of the measured far-field intensity distributions for two SNOM probes fabricated at the S.I. Vavilov State Optical Institute. Measurements were performed at a wavelength of 0.63 μm. The far-field intensities measured within the acceptance angle $\pm 87^\circ$ are presented in Figs 9a, b and 10a, b,

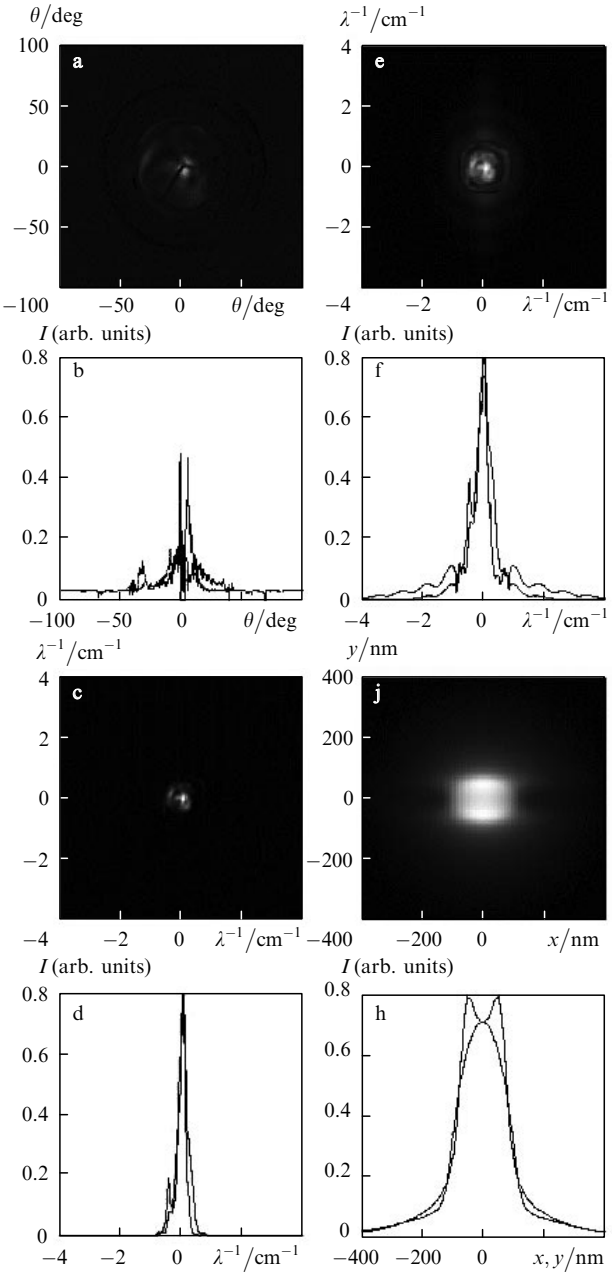

Figure 9. Illustration of the processing stages of far-field measurements for a probe with the 150-nm aperture.

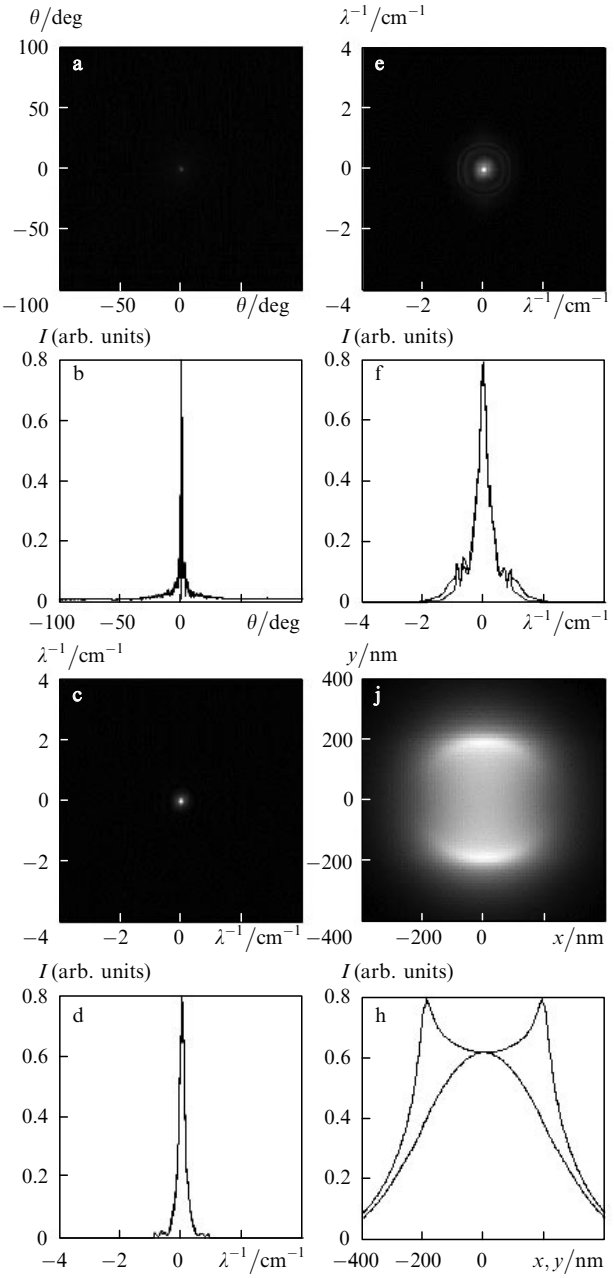

Figure 10. Illustration of the processing stages of far-field measurements for a probe with the 380-nm aperture.

respectively; the intensities obtained after the noise smoothing and reduced to the Fourier sampling are shown in Figs 9c, d and 10c, d; the analytically continued spectra are presented in Figs 9e, f and 10e, f; and the reconstructed near-field intensities are shown in Figs. 9g, h and 10g, h.

Figures 9g, h and 10 g, h present the instrumental function of the probe, which cannot be determined by non-optical methods, which excludes the possibility of using any alternative methods of probe microscopy except the method considered in this paper.

The above-presented results of the reconstruction of the near field of SNOM probes were verified directly by using a tunnelling scanning optical microscope (TSOM) at the State Optical Institute [64]. Unlike a SNOM, such a microscope operates in the photon accumulation regime, i.e. the probe does not emit but receives light reflected from a sample.

Nevertheless, TSOM experiments gave reliable estimates of the probe aperture and confirmed the achieved resolutions of 150 and 380 nm corresponding to the field parameters in Figs 9g, h and 10g, h.

Despite the positive results obtained by this method, it has theoretical and practical limitations related to many variants of the analytic continuation of the Fourier spectrum of the scalar potential $\tilde{f}_{e0}$ and the possibilities of sampling.

To perform adequate simulation, it is necessary to use the Fourier sampling of volume no less than 1024×1024. In this case, sampling intervals in the spatial and frequency domains can be made small and their number in the frequency domain will be sufficient for the complete description of the near-field and evanescent components. However, this may be not enough because to extend the definition of the evanescent components of Fourier spectra, it is also necessary to use a rather small quantisation step over the level of extremely weak signals, which may require even a greater sampling volume. For this purpose, powerful computers with parallel processors should be used.

The consequence of computational restrictions considered above is, in particular, the presence of the lower limit for the aperture diameter $2a_{\min}$ being measured, which is ~ 100 nm (or 0.15λ). The accuracy of measuring transverse dimensions of the effective near-field distribution in the aperture plane is approximately $\pm 0.6a_{\min}$ (or $\pm 0.05\lambda$).

At present nanoprobes fabricated at the State Optical Institute are being successfully tested on the setup constructed according to the scheme in Fig. 8. These probes provide the efficient operation of a TSOM-1 tunnelling scanning optical microscope. The method for control of nanoprobes proposed in the paper offers the following advantages:

(i) The absence of mechanical contacts of a probe with measuring devices, which is extremely important due to a very small diameter of the probe point (~ 150 nm);

(ii) the optical principle of obtaining information, which is necessary for the adequate estimate of the probe as a scanning tool providing the required resolution of the microscope;

(iii) the high operating efficiency of the method performing all the measurements and processing of the results for a few minutes.

Figure 11 presents images obtained with a TSOM-1 by using one of the tested probes. The horizontal and vertical resolution in these pictures is 150 nm and 10 – 100 nm, respectively, which is provided by the geometry of the probe point itself and by the feedback.

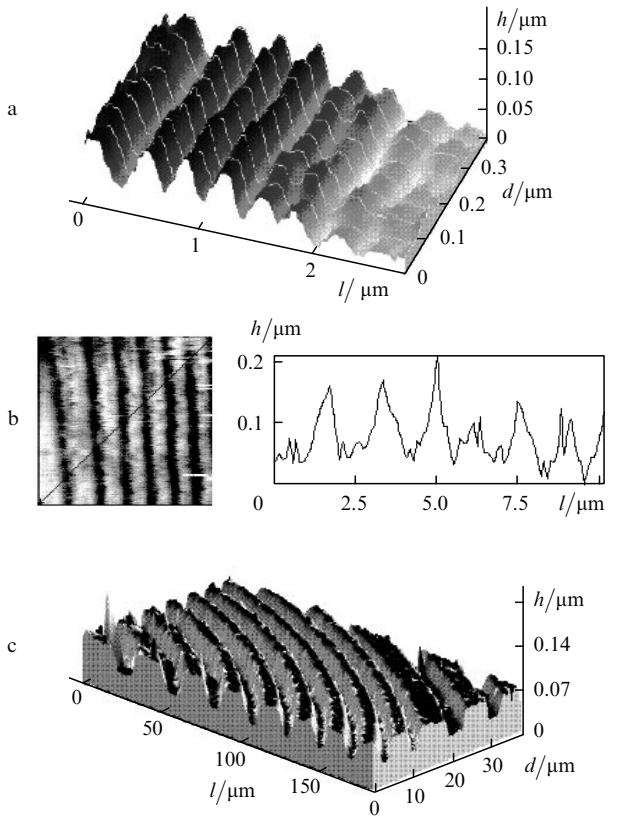

Figure 11. Image of the structure of the photothermoplastic recording (a), half-tone image and profilogram of a ruled 600-lines mm^{-1} diffraction grating (b), and topographic image of an optical disc (c) obtained with a TSOM-1 by using a tested probe.

5. Conclusions

The main problem of the development of SNOM probes is the minimisation of their aperture and increase of their transmission coefficient. The first parameter determines the possibility of imaging with a better resolution, while the second one determines the possibility of using SNOMs for local spectroscopy and surface modification. The resolution of SNOM probes is limited by the skin depth in a metal confining radiation in the probe, and it seems that the record resolution obtained in [15] can be improved only slightly. In this connection the studies devoted to the reconstruction of the optical image taking into account the size of the probe aperture and its nonlocal interaction with surfaces are important [56 – 65]. A much better resolution was obtained by using a SAFIM [12] and probably can be obtained for probes based on surface plasmons [66], where the above-mentioned restriction, which is typical for SNOM probes, is absent.

The main disadvantage of probes used at present is the presence of a transcendent region in a tapered metal waveguide where radiation decays exponentially. In a number of papers, the alternative designs of SNOM probes were proposed and realised based on two-wire transmission lines. It is known that two-wire transmission lines, including a microstripe line and a coaxial, has no the cut-off frequency for the fundamental radiation mode, which should considerably increase the transmission of optical radiation through the probe.

Probes fabricated from microstripe lines are used only for polarised light. The authors of [67] calculated the decay of light wave in a microstripe line taking into account the dispersion of the dielectric constant and conductivity of the metal. Estimates showed that the transmission coefficient of a microstripe line made of silver and having an aperture of 30 nm can achieve 60 % in the near-IR region. This result is caused by the anomalously weak decay of surface plasmons propagating along the surface of noble metals. The transmission coefficient in the visible region is much lower, but it can achieve 10 % for some materials.

A microstripe-line probe studied in [67] was made of an adiabatically tapered single-mode optical fibre covered with a two-layer metal film (vanadium and aluminium) on its opposite sides only. The transmission coefficient of such a

probe strongly depends on the direction of light polarisation (change by an order of magnitude) and its maximum value achieves a few percent (for green light). In this case, the radiation pattern of the probe is dipole for the maximum transmission (the important criterion of the probe quality) and changes for other directions of polarisation. We assume that the use of microstripes made of other metals will considerably improve the probe parameters in the near-IR region.

Another promising variant of SNOM probes based on a coaxial was proposed and realised in [68]. The probe was fabricated by using a focused ion beam and its transmission coefficient achieved unity for the aperture exceeding 200 nm.

In papers [69, 70], a tetrahedral point was used as a probe. This probe has no aperture restricting the light flux and, as a result, its resolution can achieve 10 nm. A disadvantage of the probe is that it requires the CTM rather than ATM confinement, i.e. it can be used only with conducting surfaces.

Note also that in this paper, first, we have proposed and confirmed experimentally the conception of light diffraction based on the vector description of the electromagnetic harmonic field in the inhomogeneous space by using the mathematical apparatus of the theory of linear systems and, second, have obtained the practical solution of the important and quite complicated problem of reconstruction of the parameters of subwave SNOM probes, whose aperture and near-field intensity distribution is estimated from the experimental far-field angular intensity distribution.

It is obvious that studies devoted the development and improvement of SNOM probes will be continued. In this paper, we wanted to emphasise the importance and urgency of this problem and to show the most promising, in our opinion, directions of investigations.

Acknowledgements. This work was supported by a grant of the President of the Russian Federation for the Support of Leading Scientific Schools 'Fundamentals of Laser Microtechnologies' No. NSh 5967.2006.8 and by the Russian Foundation for Basic Research (Grant No. 07-02-00887-a).

References

1. Bednorz G., Denk W., Lanz M., Pohl D.W. Eur. Patent No. 0 112 401, Int. Cl. H01J/14 (1982).
2. Lewis A., Isaacson M., Murray A., Harootunian A. *Biophys. J.*, **41**, 405 (1983).
3. Pohl D.W., Denk W., Lanz M. *Appl. Phys. Lett.*, **44**, 651 (1984).
4. Betzig E., Finn P.L., Weiner J.S. *Appl. Phys. Lett.*, **60**, 2484 (1992).
5. Durig U., Pohl D.W., Rohner F. *J. Appl. Phys.*, **59**, 3318 (1986).
6. Fisher U.Ch., Durig U.T., Pohl D.W. *Appl. Phys. Lett.*, **52**, 249 (1988).
7. Durkan C., Shvets I.V. *J. Appl. Phys.*, **83**, 1171 (1988).
8. Betzig E., Isaacson M., Lewis A. *Appl. Phys. Lett.*, **51**, 2088 (1987).
9. Courjon D., Sarayeddine K., Spayer M. *Opt. Commun.*, **71**, 23 (1989).
10. De Fornel F., Goudonnet J.P., Salomon L., Lesnievska E. *Proc. SPIE Int. Soc. Opt. Eng.*, **1159**, 77 (1989).
11. Courjon D., Bannier C. *Rep. Prog. Phys.*, **57**, 989 (1994).
12. Zenhausern F., Martin Y., Wickramasinghe H.K. *Science*, **269**, 1083 (1995).
13. Fukuzawa K., Tanaka Y. *Appl. Phys. Lett.*, **71**, 169 (1997).
14. Gresillon S., Ducourtieux S., Lahrech A., Aigouy L., Rivoal J.C., Boccara A.C. *Appl. Surf. Sci.*, **164**, 118 (2000).
15. Betzig E., Trautman J.K., Harris T.D., Weiner J.S., Kostelak R.L. *Science*, **251**, 1468 (1991).
16. Davis C.C., Atia W.A., Gungor A., Mazzoni D.L., Pilevar S., Smolyaninov I.I. *Laser Phys.*, **11**, 243 (1997).
17. Herndon M.K., Collins R.T., Hollingsworth R.E., Larson P.R., Johnson M.B. *Appl. Phys. Lett.*, **74**, 141 (1999).
18. Betzig E., Trautman J.K., Wolfe R., Gyorgy E.M., Finn P.L., Kryder M.H., Chang C.H. *Appl. Phys. Lett.*, **61**, 142 (1992).
19. Hosaka S., Kikukawa A., Koyanagi H., Miyamoto M., Nakamura K., Etoh K. *Nanotechnology*, **8**, A58 (1997).
20. Zeisel D., Dutoit B., Deckert V., Roth T., Zenobi R. *Anal. Chem.*, **69**, 749 (1997).
21. Naber A., Dziomba T., Ficher U.C., Maas H.-J., Fuchs H. *Appl. Phys. A*, **70**, 227 (2000).
22. Dryakhlushin V.F., Klimov A.Yu., Rogov V.V., Shashkin V.I., Sukhodoev L.V., Volgunov D.G., Vostokov N.V. *Nanotechnology*, **11**, 188 (2000).
23. Herndon M.K., Collins R.T., Hollingsworth R.E., Larson P.R., Johnson M.B. *Appl. Phys. Lett.*, **74** (1), 141 (1999).
24. Smolyaninov I., Mazzoni D.L., Davis C.C. *Appl. Phys. Lett.*, **67**, 3859 (1995).
25. Davy S., Spajer M. *Appl. Phys. Lett.*, **69**, 3306 (1996).
26. Massanell J., Garcia N., Zlatkin A. *Opt. Lett.*, **21**, 12 (1996).
27. Maheswari R. Uma, Tatsumi H., Katayama Y., Ohtsu M. *Opt. Commun.*, **120**, 325 (1995).
28. Nagahara L.A., Yanagi H., Tokumoto H. *Nanotechnology*, **8**, A50 (1997).
29. Martin Y., Zenhausern F., Wickramasinghe H.K. *Appl. Phys. Lett.*, **68**, 2475 (1996).
30. Crowell P.A., Young D.K., Keller S., Hu E.L., Awschalom D.D. *Appl. Phys. Lett.*, **72**, 927 (1998).
31. Guenther T., Emiliani V., Intonti F., Lienau C., Elsaesser T. *Appl. Phys. Lett.*, **75**, 3599 (1999).
32. Chaves-Pirson A., Temmyo J., Kamada H., Gotoh H., Ando H. *Appl. Phys. Lett.*, **72**, 3494 (1998).
33. Matsuda K., Saiki T., Saito H., Nishi K. *Appl. Phys. Lett.*, **76**, 73 (2000).
34. Richter A., Subtitz M., Heinrich D., Lienau Ch., Elsaesser T., Ramsteiner M., Notzel R., Ploog K.H. *Appl. Phys. Lett.*, **73**, 2176 (1998).
35. Unlu M.S., Goldberg B.B., Herzog W.D., Sun D., Towe E. *Appl. Phys. Lett.*, **67**, 1862 (1995).
36. Herzog W.D., Unlu M.S., Goldberg B.B., Rhodes J.H., Harder C. *Appl. Phys. Lett.*, **70**, 688 (1997).
37. Dryakhlushin V.F., Klimov A.Yu., Rogov V.V., Filatov D.O., Kruglov A.V. *Poverkhnost'*, **15**, 64 (2000).
38. Kim J., Boyd J.T., Jackson H.E., Choquette K.D. *Appl. Phys. Lett.*, **76**, 526 (2000).
39. Smolyaninov I.I., Mazzoni D.L., Mait J., Davis C.C. *Phys. Rev. B*, **56**, 1601 (1997).
40. Smolyaninov I.I., Zayats A.V., Davis C.C. *Phys. Rev. B*, **56**, 9290 (1997).
41. Valaskovich G.A., Holton M., Morrison G.H. *Appl. Opt.*, **34**, 1215 (1995).
42. Dryakhlushin V.F., Klimov A.Yu., Rogov V.V., Gusev S.A. *Instrum. Experim. Techniques*, **41** (2), 138 (1998).
43. Zeisel D., Nettesheim S., Dutoit B., Zenobi R. *Appl. Phys. Lett.*, **68**, 2491 (1996).
44. Radmacher M., Hillner P.E., Hansma P.K. *Rev. Sci. Instrum.*, **65**, 2737 (1994).
45. Danzebrink H.U., Wilkening G., Ohlsson O. *Appl. Phys. Lett.*, **67**, 1981 (1995).
46. Akamine S., Kuwano H., Yamada H. *Appl. Phys. Lett.*, **68**, 579 (1996).
47. Kalachev A.I., Smirnov I.B., Veiko V.P., et al. *Proc. SPIE Int. Soc. Opt. Eng.*, **3822**, 199 (1999).
48. Atlasov K.A., Veiko V.P., Kalachev A.I., Kaporskii L.N., Yakovlev E.B. *Izv. Ros. Akad. Nauk, Ser. Fiz.*, **65**, 941 (2001).
49. Williamson R.L., Miles M.J. *Appl. Phys.*, **80** (9), 4804 (1996).
50. Snopko V.N. *Osnovy metodov pirometrii po spektru teplovogo izlucheniya* (Fundamentals of the Methods of Pyrometry by the Thermal Emission Spectrum) (Minsk: B.I. Stepanov Institute of Physics, 1999).

51. Ribaut G. *Opticheskay pirometriya* (Optical Pyrometry) (Moscow: GTTI, 1934).
52. Yatsui K., Itsumi K., Kourogi M., Ohtsu M. *Appl. Phys. Lett.*, **80**, 2257 (2002).
53. Saiki Ç., Matsuda K. *Appl. Phys. Lett.*, **74**, 2773 (1999).
54. Born M., Wolf E. *Principles of Optics* (Oxford: Pergamon Press, 1969; Moscow: Nauka, 1973).
55. Veiko V.P., Voznesenskii N.B., Voronin Yu.M., Rodionov S.A., Smirnov I.B., Kalachev A.I. *Izv. Ros. Akad. Nauk, Ser. Fiz.*, **63**, 1954 (1999).
56. Veiko V.P., Voronin J.M., Voznessenski N.B., Rodionov S.A., Smirnov I.B., Kalachev A.I. *Proc. SPIE Int. Soc. Opt. Eng.*, **3688**, 406 (1999).
57. Voznesenskii N.B., Ivanova T.V., Vonogradova G.N. *Opt. Zh.*, **65**, 43 (1998).
58. Voznesenskii N.B., Rodionov S.A., Domnenko V.M., Ivanova T.V. *Abstracts of Papers, Mezhdunarodnaya konf. 'Prikladnaya optika-96'* (International Conference on Applied Optics-96) (St. Petersburg, LITMO, 1996).
59. Voznesenskii N.B., Rodionov S.A., Domnenko V.M., Ivanova T.V. *Opt. Zh.*, **64**, 48 (1997).
60. Vozneseskii N.V., Ivanova T.V. *Sbornik meterialov Vserossiiskogo soveshchaniya 'Zondovaya mikroskopiya-2000'* (Collection of Papers, All-Russian Conference on Probe Microscopy-2000 (Nizhnii Novgorod, 2000) p. 326.
61. Veiko V.P., Voznesenskii N.B., Gusev A.E., Ivanova T.V., Rodionov S.A. *Opt. Zh.*, **65**, 49 (1998).
62. Veiko V.P., Voznessenski N.B., Domnenko V.M., Ivanova T.V., Rodionov S.A., Goussev A.E. *Proc. SPIE Int. Soc. Opt. Eng.*, **3467**, 313 (1998).
63. Veiko V.P., Voznessenski N.B., Domnenko V.M., Ivanova T.V., Rodionov S.A., Goussev A.E. *Proc. SPIE Int. Soc. Opt. Eng.*, **3736**, 341 (1999).
64. Voronin Yu.M., Voznesenskii N.B. *Opt. Zh.*, **65**, 94 (1998).
65. Gaikovich K.P., Dryakhlushin V.F., Kruglov A.V., Zhilin A.V. *Phys. Low-Dim. Struct.*, **5/6**, 93 (2002).
66. Gurevich V.S., Libenson M.N. *Ultramicroscopy*, **57**, 77 (1995).
67. Dryakhlusin V.F., Klimov A.Yu., Rogov V.V. *Poverkhnost'*, **15**, 40 (2000).
68. Kassing R. *Proc. Int. Workshop 'Scanning Probe Microscopy-2002'* (Nizhny Novgorod, 2002) p. 52.
69. Koglin J., Fischer U.C., Fuchs H. *Phys. Rev. B*, **55**, 7977 (1997).
70. Ferber J., Fischer U.C., Hagedorn N., Fuchs H. *Appl. Phys. A*, **69**, 581 (1999).